CFD simulation with experimental validation of oil-water core-annular flows through Venturi and Nozzle flow meters

Parham Babakhani Dehkordi[*], Luigi Pietro Maria Colombo, Manfredo Guilizzoni, Giorgio Sotgia

Politecnico di Milano - Department of Energy, via Lambruschini 4, 20156, Milano, Italy

In the present study, Volume of Fluid (VOF) multiphase flow model by ANSYS Fluent 16.2 is used to characterize core-annular flow patterns of highly-viscous oil-water flows through a Venturi Flow Meter (VFM) and a Nozzle Flow Meter (NFM) in a 40 mm i.d. horizontal pipe. Numerical simulations are compared with experiments, for oil superficial velocities in the range 0.25–0.75 m s^{-1} and water superficial velocities in the range 0.44–1.32 m s^{-1}. Eight cases were considered for numerical runs. Two turbulence models were considered, namely realizable $k-\varepsilon$ and Shear Stress Transport (SS) $k-\omega$. Two phase pressure drop, instantaneous radial velocity and holdup profile, cross-sectional time-averaged holdup and slip ratio were extracted from CFD simulations. Flow patterns were also compared to actual images taken by a Olympus E-M10 mirrorless camera. In terms of concentrated pressure drop and mean water holdup, the results of CFD simulations are consistent with the experimental data. Prediction of the total mass flow rate, computed by homogeneous model, for both the VFM and NFM also gave very satisfactory results.

Keywords: Venturi flow meter, Nozzle flow meter, Core-annular flow, CFD simulation

1. Introduction

The world energy demand is still satisfied for its large majority by fossil fuels and continuous research is active to find and exploit new reservoirs, in order to increase both the available resources and the world areas and countries having access to significant assets. Over the last years the oil and gas sector has given an increasing attention to the so-called transitional oils and unconventional oils. The latter have been defined in different ways, but in summary they can be classified as two groups of liquid hydrocarbons, from different sources, that are characterized by higher densities, viscosities, sulfur and impurities contents than the conventional oil, and that cannot be extracted, transported and processed using conventional techniques (IEA, 2013; Gordon, 2012). With respect to the conventional oils and the natural gas, the total amount of transitional and unconventional oils is larger and the reserves are distributed in a higher number of nations. Counterposed to these advantages, transitional and unconventional oils also pose new challenges. Particularly, transitional oils are difficult to extract, but they can be then transported and processed by conventional techniques; on the contrary, transport of unconventional oils is problematic too, due to their high densities and particularly high viscosities. To make the pipeline transport of unconventional oil feasible, commonly used solutions are dilution, heat treatment and partial upgrading, while emulsion and Core Annular Flow (CAF) are

under study and development (Saniere et al., 2004). Using the latter two solutions, oil is mixed with water to reduce its equivalent viscosity and the resulting pumping power, and between the two the setup of a CAF seems particularly promising from the point of view of this reduction thanks to the lubricating effect of the water liquid film, that prevents oil contact with the pipeline wall (Oliemans and Ooms, 1986; Joseph et al., 1997; Sotgia et al., 2008). In fact, in this flow regime water moves adjacent to the pipe wall while oil flows as the inner core, resulting in reducing wall shear stresses and lowering two phase pressure drop. This favorable flow pattern only occurs for suitable flow rates of the phases, so further relevance is added to the issue – already of great importance for the conventional oil and gas industry – of predicting and measuring the mass flow rates of the phases and of the total mixture. Many different solutions for this measurement were described in the literature and proposed for patents. A primary distinction is between devices that can monitor multiphase flow inline and meters that requires flow spill and phase separation. The first ones can be simply mounted on the production facilities and they are much cheaper alternatives to multiphase separators, also in terms of operational costs. Within the family of the inline measurement tools, the most used principle is the attenuation of single- or dual-energy γ-rays, with all the related issues and costs. Devices based on the electrical permittivity of the mixture, on microwaves or ultrasounds, turbine and vortex flow- meters, and combination of the previous were also

---

[*] Corresponding author
 E-mail address: Parham.babakhani@polimi.it (P. Babakhani Dehkordi).

Published Journal Article available at: http://dx.doi.org/10.1016/j.petrol.2016.10.058

proposed (Falcone et al., 2009; NFOGM, 2005). Another type of metering devices is the one based on differential pressure measurements, including Venturi Flow Meters (VFM) and Nozzle Flow Meters (NFM). These can be of great practical interests for oil and gas industries because they have no moving part, thus greatly reducing (virtually to none) the need for maintenance (Atkinson et al., 2004), but an issue in the use of these meters is that they have to rely on models to link the measured pressure difference to the mass flow rates. Thus, it is necessary to characterize in detail multiphase flow across these devices.

2. Literature review

Both experimental and numerical studies about flows through measuring devices can be found in the literature, but the majority of them are related to gas-liquid flows, and particularly to the so-called "wet-gas", i.e. the flow of a low mass flow rate of liquid in gas main stream. As significant examples, the papers by Chisholm (1967), Leeuw (1997) and Oliveira et al. (2009) can be cited. Chisholm (1967) developed a model to estimate pressure drop across orifices during flows of incompressible two-phase mixtures. Concentrated pressure from the upstream tube to the throat section is correlated to the mixture mass flow rate by a Lockhart-Martinelli parameter. The work by Leeuw (1997) deals with two-phase flows of gas-liquid through a Venturi meter, developing an empirical correlation that shows dependence of the mixture mass flow rate on the gas Froude number. The relative error in the mixture mass flow rate between predictions by the correlation and experimental data is less than 2%. Oliveira et al. (2009) measured mass flow rates related to wet gas flows using a resistive void fraction meter and a Venturi or Orifice plate meter. Upward vertical and horizontal pipes were considered for this purpose, including bubbly, annular, churn and slug flow regimes. The duct inclination, and therefore gravity, is found to exert a negligible influence on the frictional pressure, and a slip ratio lower than 1.1 is predicted for bubbly and slug flow regime. Additional references to papers dealing with gas-liquid flows across a Venturi meter can be found in the paper by Jana et al. (2008).

Concerning liquid-liquid flows that will be the subject of the present work through measuring devices, there are much less papers and information is still partially lacking. The work by Pal (1993) deals with the application of the Venturi and Orifice flow meter to monitor the flow rate of water/oil emulsion in presence of surfactant. Oil concentration varied over wide range of 0–84.32 vol%. They developed an empirical correlations based on their experimental data for discharge coefficient of the Venturi and Orifice flow meter. Skea and Hall (1999) evaluated oil-water flows in single-phase flow meters, considering water-in-oil and oil-in-water emulsions. Water with oil (kinematic viscosity=$1 \cdot 10^{-5}$ m^2/s at 50 ℃) fraction up to 15% and oil with water fraction up to 15% were considered as mixtures. Different devices were tested including 50.8 mm (2-in.) and 101.6 mm (4-in.) positive displacement meters, turbine and Venturi meters. Single phase flow meters turned out to be suitable for oil-water emulsions showing a maximum error within 1% of the reference total volume flow rate. Oddie and Pearson (2004) reviewed the most important techniques for gas-liquid, gas-solid, liquid-solid and liquid-liquid flows to measure mixture flow rates using combinations of multiphase flow devices for both horizontal and vertical pipes. They emphasized the importance of the flow regime to select an appropriate multiphase flow meter. The work by Li et al. (2009) deals with development of a hybrid flow meter for measurement of oil-water two-phase flow. Three Venturi meters and three oval gear flow meters were introduced for this purpose. Three pipe diameters equal to 15 mm, 25 mm and 40 mm was selected to measure the total flow rate ranging from 1.2 m^3 h^{-1} to 5.5 m^3 h^{-1}. Tap water and diesel oil with density 847.95 kg m^{-3} were used. Different throat/inlet area ratios were tested, namely 0.74 for the 15 mm i.d. tube, 0.68 for the 25 mm i.d. tube and 0.58 for the 40 mm i.d. tube.

Mass flow rate is correlated to two phase pressure drop (between upstream pipe and throat section) by a coefficient k referred to the calibration coefficient of the Venturi meter. Thus, two calibration coefficients k_{water} and k_{oil} are defined, whose numerical values are obtained based on single phase flows. k_{water} is slightly different from k_{oil}, with the difference more significant for low volume flow rates. The conclusion is that when oil fraction is less than 40%, k_{water} must be used. On the contrary, in flow conditions associated with oil fraction higher than 60%, k_{oil} has to be considered. An average calibration coefficient is chosen for oil fraction between 40% and 60%. It is worth noting that both oil fraction and selection of calibration coefficient has a considerable influence on the results. Tan and Dong (2010) proposed a new correlation to take into account the effect of oil viscosity of water-oil through a V-cone multiphase flow meter. Superficial velocity of oil and water were varied in the ranges 0–3.6 m s^{-1} and 0.63–1.69 m s^{-1}, respectively. A low-viscosity oil was selected and the flow regime was emulsion oil/water and emulsion water/oil. A comparison of experimental data with homogeneous and separated flow models was performed, evidencing that the total mass flow rate predicted by the homogeneous model shows a lower root mean square (RMS) deviation as compared to the separated model, which seems consistent with the flow structure.

Specifically concerning core annular flow, necessary conditions for a CAF to be possible are high viscosity of oil and small density difference between water and oil (Charles, 1961; Angeli and Hewitt, 2000). Given the importance of such flow regime, many studies were devoted to it. An historical review of this topic, with references to the most important papers, can be found in the book by Joseph and Renardy (1993). A theoretical analysis of core-annular flow of very high viscos oil-water was studied by Ooms et al. (1984). They developed a model based on hydrodynamic lubrication theory. Two test sections with the diameters of 50.8 mm and 203.2 mm was considered. . Pressure drop predicted by the model was compared with measurements showing satisfactory agreement.

Oliemans et al. (1987) performed tests regarding to core flow of high viscous oil (3 Pa s) and water in a 50 mm test facility to capture information concerning the amplitude and length of waves at the oil/water interface. They emphasized the importance of turbulence in water film on pressure calculation. Detection of flow patterns and measurement of pressure drop for seven different Pyrex and Plexiglas pipe diameters were performed by Sotgia et al. (2008). Oil with viscosity μ_o=910 Pa s at 20 ℃ and tap water were used, giving a density ratio of 0.9 between the two fluids. Experimental two phase pressure reduction factor were compared with the models by Arney et al. (1993) and Brauner (1991). The two models showed good agreement with the data for core annular flow. Colombo et al. (2012) developed a semi-empirical model to identify the critical transition from annular to wavy-stratified flow.

Concerning CFD simulation, Ghosh et al. (2010) and Kaushik et al. (2012) performed numerical analysis on oil-water core-annular flows in downward vertical flows and horizontal, respectively. The predicted pressure drop is in a satisfactory agreement with actual data.

The above literature reveals that detailed information about core-annular flow of high viscous oil-water through VFM and NFM measuring devices is lacking. The aim of the present research is therefore double. The first aim is to investigate if two-phase CFD analysis, validated through a comparison with experimental data, can be a reliable tool to investigate VFMs and NFMs and can offer significant insight about the behavior of highly viscous oil-water flows in such devices. If so, CFD would candidate as a valuable engineering tool for the design and use of these devices in all those situations, quite common in the oil and gas fields, where experiments may be too complex or time consuming. The second aim is to assess the performance of VFMs and NFMs in the prediction of the flow rates of a heavy, highly viscous oil-water mixture in Core Annular Flow.
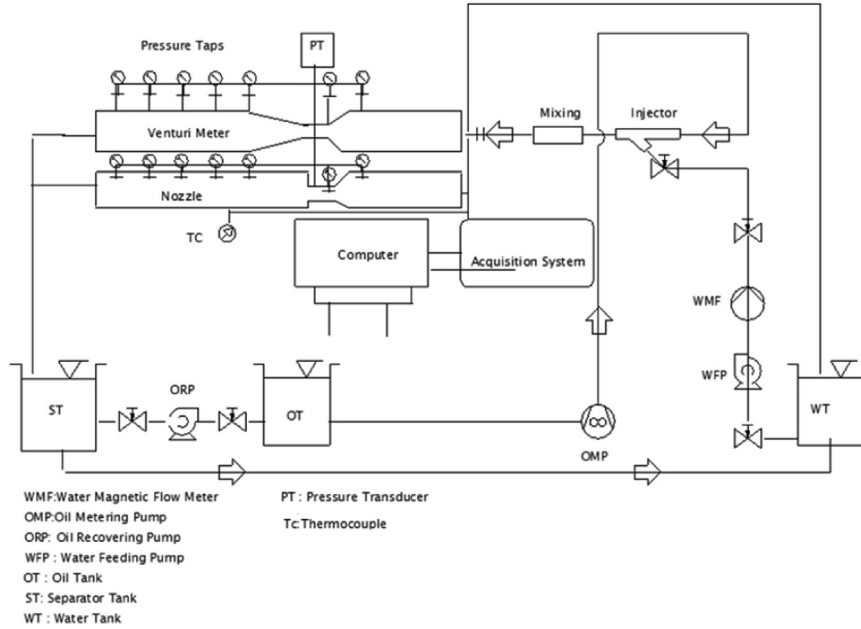
Fig. 1. Schematic representation of test facility.

3. Experimental facility and procedures

Brief overviews about the fundamental governing parameters for two-phase flow and the basic theory of differential pressure measurement devices can be found in Appendices A and B, respectively. Here the experimental rig and the procedure followed for the experimental tests will be described.

The sketch of the experimental test section is shown in Fig. 1. A detailed description of the setup can be found in Sotgia et al. (2008). Magnetic flow meter (accuracy ± 0.5% of the reading) is used to measure the water flow rate, while a calibrated metering pump is used for pumping oil. To facilitate the onset of core-annular flow, oil (Milpar 220, ρ_o=910 kg m^{-3}, μ_o=0.9 Pa s at 20 °C) and tap water (ρ_w=998 kg m^{-3}, μ_w=1.026 × 10^{-3} Pa s) are injected in the test section through a co-axial mixer, with water in the annulus and oil in the core. The test section is composed of 11 m of transparent Plexiglas tubes (to be able to visualize flow patterns), positioned horizontally with the VFM or NFM installed near the half of the test section length. Both upstream and downstream pipes have an internal diameter of 40 mm. The VFM and NFM were manufactured according to the indications of the ISO standard (ISO, 5167-4, 2003), with a throat diameter of 30 mm. A differential pressure transducer (SETRA model 230, with full scale 6.89 kPa (1 psi), accuracy ± 0.5% of the full scale) and a K type thermocouple were used to measure pressure drop and mixture temperature, respectively. Monitoring mixture temperature is necessary because oil viscosity is highly temperature sensitive. The high pressure tap is installed in the upstream tube, 5 mm before the beginning of the convergent section, while the low pressure tab is mounted at the throat section. The distance between the upstream and throat pressure taps is 30 mm.

Separation between the phases after the test section is by gravity, so it requires some time; as a consequence tests cannot be run continuously: they have to be stopped when all the oil and water in the feeding tanks are moved to the separator tank. Thus, tests were organized in series, characterized each by a fixed value of the oil mass flow rate. The experimental procedure to perform them is thus as follows: single-phase water flow with the maximum superficial velocity $J_{w,max}$ to be investigated in the series is introduced into the test section, then oil is injected at the superficial velocity J_o that characterizes the series. Then, single tests are performed, decreasing J_w at each run until it reaches the minimum value of interest. After separation of the phases, oil superficial velocity is changed and a new series can be

acquired. In addition to visual inspection, recording of the flow patterns was performed using a Olympus E-M10 mirrorless camera with exposure time 1/4000 s. The summary of experimental conditions is reported in Table 1. A total of 45 and 36 experimental data points were considered for the VFM and the NFM, respectively Experimental tests cover a range of flow patterns including dispersed, core-annular (concentric and eccentric, with and without drops) regimes.

Among them, eight representative cases have been selected for numerical analysis. Fig. 2 reports them in a flow pattern map resulting from previous experimental campaigns. The simulated conditions include six core-annular flow cases, two core-annular wavy flow cases (i.e. near to the transition from core-annular to stratified flow). Dispersed flow pattern has not been taken into account because the interface length scale is much smaller, in some cases near to being comparable with the cell size, thus Volume-of-Fluid models would not be a suitable choice for simulation.

Table 1
Summary of experimental conditions.

J_0 (m s^{-1})	J_W (m s^{-1})	Re_{so}	Re_{sw}
0.25–0.75	0.44:0.22:1.32	11–32	18–53·10^3

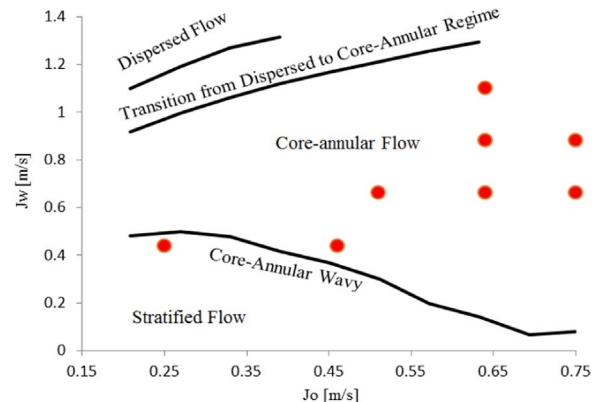**Fig. 2.** Flow pattern map, resulting from previous experimental campaigns (Colombo et al., 2012) with indication of the flow condition simulated in the present work.

4. Numerical multiphase model

4.1. Volume of Fluid (VOF)

In the CAF flow pattern, the two phases are immiscible and separated by an interface having a length scale comparable to the pipe diameter (particularly for the oil core, but also for the larger oil drops). Such interface is continuously varying in terms of shape and extension, due to the constant evolution of the flow structures. In the field of CFD analysis, these are conditions for which numerical methods based on the Volume of Fluid (VOF) (Hirt, 1981) are among the most suitable (Ranade, 2002). The latter were originally developed and used in other two-phase fields (drop impacts, sloshing tanks), but examples of their use for two-phase flow are already reported in the literature (Ghosh et al., 2010; Kaushik et al., 2012; Desamala et al., 2016). Combined methods (e.g. Menard, 2007) would also be very well-suited, but they are also much more complex and no ready-to-use solver is available, so that their use is at present restricted to academic studies. Euler-Euler models (e.g. Vallee et al., 2008) may give good results too, but they lack the interface tracking offered by the VOF approach.

Therefore, VOF was selected for this study and simulations were performed on 3D domains using the VOF method implemented in the CFD code ANSYS Fluent 16.2. The software was used with no modification or addition by user defined functions, as one of the aims was to evaluate its performances as it is. An overview about the VOF method is given in Appendix C, while all the modeling choices adopted for the present study will be described in the following subsections.

4.2. Turbulence models

As it is evident from Table 1, the oil phase is always in laminar motion, while the flow of water remains turbulent. Therefore, two Reynolds-Averaged Navier-Stokes (RANS) turbulence models were selected for the simulations: Realizable $k - \varepsilon$ (RKE) model and Shear stress transport (SST) $k - \omega$ scheme (with turbulence damping at interface) to compare their performances. All the details and the mathematical derivations for both models can be found in Varsteeg and Malalasekera (1995). As suggested by Ghosh et al. (2010), monitoring cross sectional contour of turbulent viscosity at different axial location reveals that in the core the viscosity is close to molecular viscosity of oil, while in the annulus the viscosity is significantly larger than the molecular viscosity of water. This indicates that the model is able to maintain oil in laminar conditions and water in turbulent regime in the corresponding regions.

4.3. Computational geometry

A 3D shaded rendering of the flow domains is shown in Fig. 3. They reproduce the geometries that have been experimentally tested. The diameter ratio (β) of the VFM and NFM is 0.75, with upstream and downstream pipe diameters of 40 mm and a divergent angle of 7.5° for
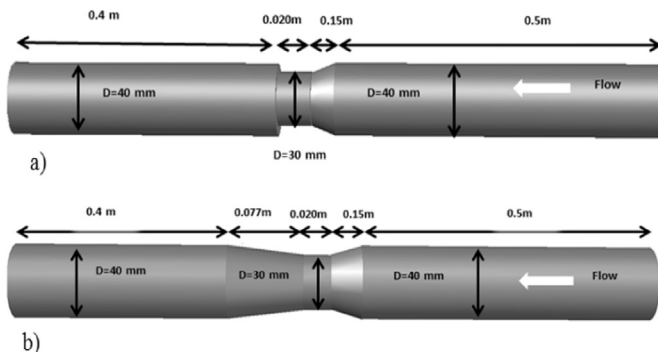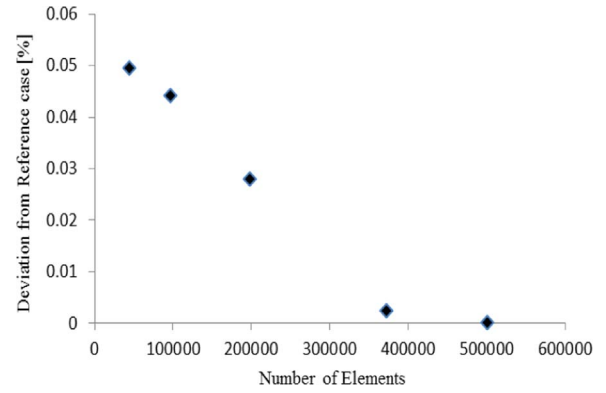
Fig. 4. Grid independence analysis on the two-phase pressure drop.

both devices. Unlike the VFM, the NFM encounters a sudden change of cross section after throat section. Upstream and downstream pipes were modeled with a length of 500 mm and 400 mm as a compromise between the need to allow flow development and the computational expense. Computational domain was meshed using hexahedral elements as they grant both a reduction in the volume element count and superior accuracy and convergence to solution. In order to verify grid independence of the results, two phase pressure drop for the finest used mesh (500,871 elements) is considered as a reference and percentage deviation from such reference is plotted in Fig. 4. The results presented in the following are all from the simulations with 500,871 elements. Such a mesh can be considered as still quite coarse and it was selected to keep the simulation time reasonably short
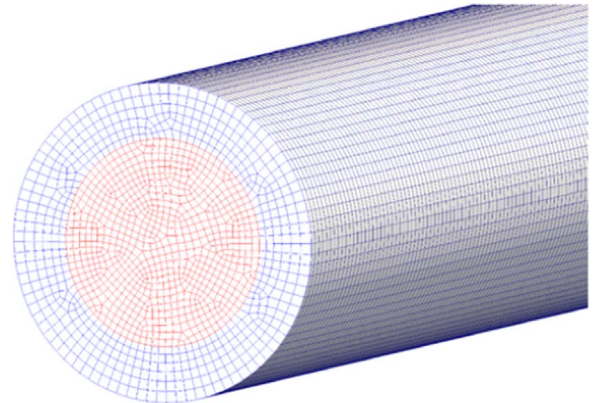
Fig. 5. Injection of oil and water into domain: oil is injected from the core, while water is injected circumferentially. Red and blue colors indicate oil and water regions, respectively. (For interpretation of the references to color in this figure legend, the reader is referred to the web version of this article.)
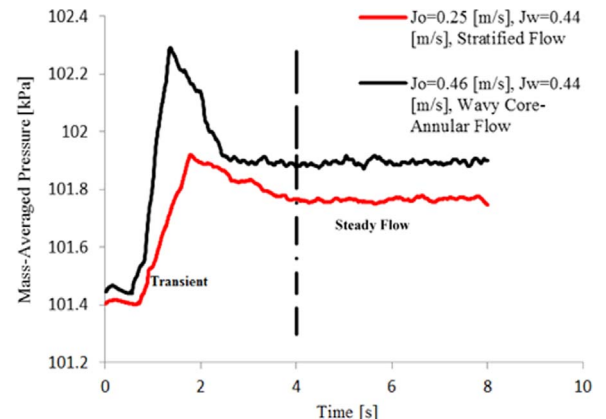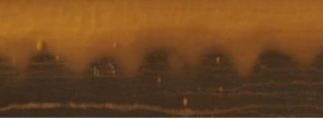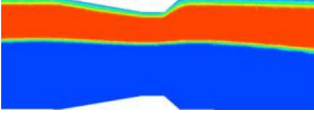
Fig. 3. Sketch of 3D geometries of a) NFM and b) VFM.
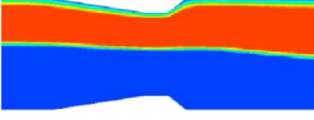
Fig. 6. Cross-sectional time-averaged pressure at L=0.495 m from inlet for the VFM.

Table 2
Flow patterns experimentally observed and calculated by the simulations.

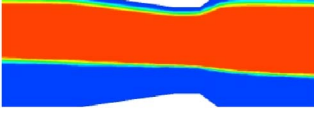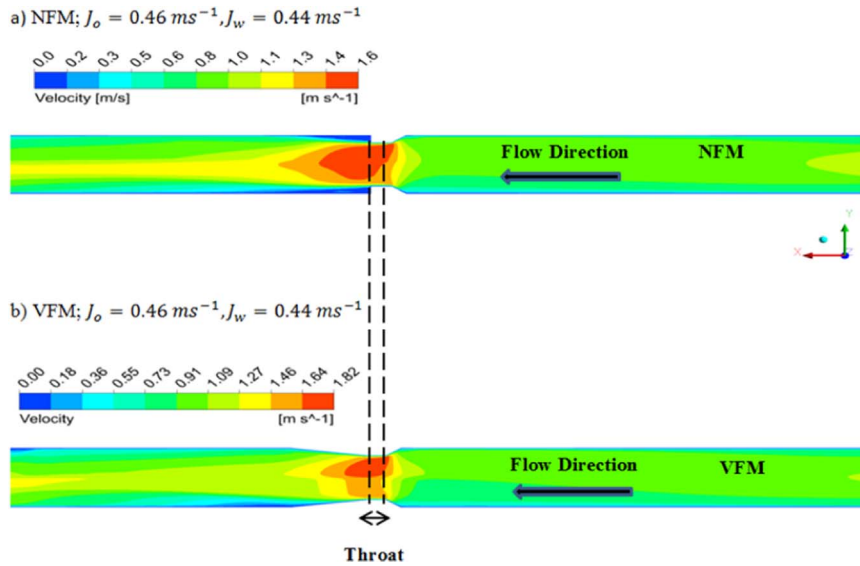| Experimental observation (Upstream of throat section)	Experimental observation (Throat section)	CFD prediction (Throat section)	J_o (m s^{-1})	J_w (m s^{-1})	Flow regime
			0.25	0.44	Core-annular wavy
			0.46	0.44	Core-annular wavy
			0.75	0.66	Perfect Core-annular

Fig. 7. Velocity contour in the vertical axial plane for a) NFM and b) VFM.

(indicatively less than one week) also on common hardware (desktop or laptop PC). One of the aims of the study is in fact to verify if numerical simulation can be a suitable tool for analyzing multiphase flow also from an industrial point of view, in situations where time is often a very scarce resource.

4.4. Initial and Boundary condition

Computational domain is initially filled with water as in the experimental conditions, then the two fluids are separately injected into the domain. As it is evident from Fig. 5, oil is injected from the core of the inlet cross-section (part of the mesh colored in red), while water is injected circumferentially (part of the mesh colored in blue). To ensure that the velocities imposed at the inlet surfaces for oil and water are the same as in the experiments, constant and uniform velocity is obtained as

$$U_{o,inlet} = \frac{J_o}{H_o} \tag{1}$$

$$U_{w,inlet} = \frac{J_w}{H_w} \tag{2}$$

where H_w is calculated according to the Arney et al. (1993) correlation

$$H_w = \varepsilon_w [1 + 0.35(1 - \varepsilon_w)] \tag{3}$$

The latter was checked in previous works as providing a very good agreement with the experimental data, see for instance Arney et al. (1993) and Colombo et al. (2015). No-slip conditions and zero gauge pressure are considered for the duct wall and the duct outlet, respectively.

4.5. Numerical procedure

The governing transport equations were discretized using the finite-volume method. Three-dimensional transient simulations were carried out because of the natural variation in time and space of the multiphase flow phenomena. Concerning continuity equation and pressure-velocity coupling, the PRESTO and PISO algorithms, originally developed
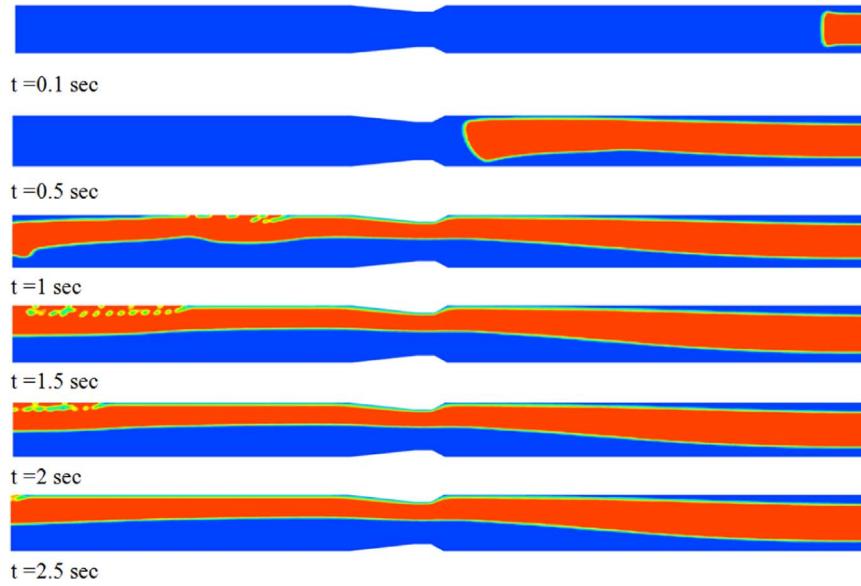
Fig. 8. Development of the oil core phase through the VFM at different time steps, for the flow pattern corresponding to J_O=0.46 m s^{-1}, J_W=0.44 m s^{-1}.

by Patankar (1980) and Issa (1986), were used. The second order upwind method was used for momentum, turbulent kinetic energy and dissipation rate. Geo-reconstruction method was adopted for the volume fraction equation and interface reconstruction. Time step is selected as 0.0001 to respect to Courant number criterion, based on the mesh size and an estimated maximum velocity in the domain. Numerical convergence was decided when the residuals of continuity are lowered three orders of magnitude, while for momentum, turbulence and volume fraction equations four order of magnitudes were considered. Fig. 6 indicates the results of time monitoring of cross-sectional average pressure regarding to VFM at upstream pipe location of L=0.495 m, for two cases: wavy core-annular flow (J_O=0.25 m s^{-1}, J_W=0.44 m s^{-1} and J_O=0.46 m s^{-1}, J_W=0.44 m s^{-1}).

At early times of simulation, the average pressure of the cross-section is low due to the fact that only water is present in the domain. As soon as oil flows through the domain, average pressure increases and pressure fluctuation is high until time t=4 s, since which very low variation of average pressure with respect to run time is observed. Thus, stabilized solution can be assumed after t=4 s.

5. Result and discussion

5.1. Qualitative analysis

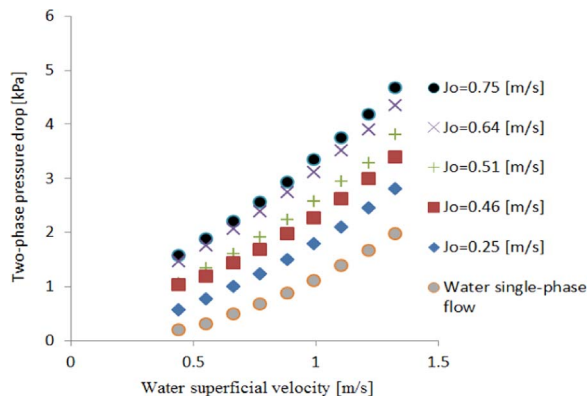Table 2 reports a qualitative comparison between three experi-

mental and numerically predicted flow patterns in the VFM. The color scale is from blue (representing water) to red (representing oil), with intermediate colors evidencing the evolution of the VOF color function in the interface region. For the flow conditions under investigation, VOF model is able to capture the macroscopic behavior of the oil core, the presence of a very thin layer of water over the core (also in the throat section of the VFM), the core eccentricity and the shape of its cross-section, the difference between thin and thick oil cores that was already observed by Kaushik et al. (2012). On the contrary, it is not able to reproduce the corrugations and waves of the oil-water interface, likely due also to the use of an averaged (RANS) approach. For the cases of wavy core-annular flow, it is experimentally observed that the interfacial waves disappear when the mixture flows through the throat section, likely due to the acceleration that induces a transition to core annular flow. Thus the flow behavior at the throat section is well reproduced by the CFD simulation.

The velocity contours of the fluid stream in the vertical axial plane of the NFM and the VFM for J_O=0.46 m s^{-1}, J_W=0.44 m s^{-1} are shown in Fig. 7a and b, respectively. The velocity magnitude is also mentioned beside each figure. Obviously, maximum velocity is reached in the throat section in both cases, however, it lasts for a longer distance for the NFM than the VFM. This might be due to the mixing zone and turbulence effect after the sharp expansion in the case of the NFM.

Fig. 8 reports the transient relative to the development of the oil
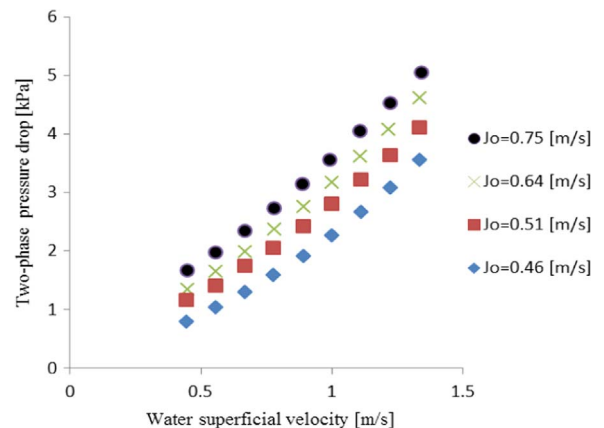

Fig. 9. Experimental concentrated pressure drop in the VFM as a function of water and oil superficial velocities.

Fig. 10. Experimental concentrated pressure drop in the NFM as a function of water and oil superficial velocities.

Table 3
Comparison of two phase pressure drop using different turbulence models for the NFM.

J_0 [m s^{-1}]	J_W [m s^{-1}]	Numerical ΔP RKE [kPa]	Numerical ΔP SST ($k-\omega$) [kPa]	Experimental ΔP [kPa]	Relative deviation (%) for RKE	Relative deviation (%) for SST ($k-\omega$)
0.46	0.44	0.78	0.79	0.79	0.91	1.1
0.51	0.66	1.45	1.39	1.735	16.4	19.4
0.64	0.66	1.72	1.64	1.985	12.8	17.3
0.64	0.88	2.41	2.29	2.75	12.0	16.7
0.64	1.10	3.17	3.01	3.61	12.1	16.3
0.75	0.66	2.07	1.95	2.34	11.2	16.5
0.75	0.88	2.72	2.57	3.14	13.3	18.0

core in the VFM for a typical core-annular flow pattern (J_0=0.46 m s^{-1}, J_W=0.44 m s^{-1}). At the early time of simulation, fouling phenomenon occurs downstream of the VFM. This situation must be avoided in practical application because it can significantly increase pressure drop due to the oil contact at the wall. However, a thin layer of water is observed at the time higher than 2.5 s showing that the situation rapidly evolves towards a fully core annular, though strongly eccentric, flow pattern.

5.2. Pressure drop

5.2.1. Experimental two phase pressure drop

At least three measurements of the two phase pressure drop have been performed for each experimental condition: the overall standard deviation is 3.2% for the VFM and 4.1% for the NFM, assessing the good repeatability of the measurements. Figs. 9 and 10 show the actual concentrated two-phase pressure drop for the VFM and the NFM horizontally operated, as a function of water superficial velocity and with oil superficial velocity as a parameter. Single-phase water flow and oil-water two-phase flow with J_0=0.25 m/s was only experimentally tested for the VFM.

As expected, for fixed amount of water, increase of oil content results in larger pressure drop, as well as, keeping oil superficial velocity constant, addition of water increases the pressure drop. Very regular trends are observed in both cases. These experimental results represent the benchmark data for the simulations.

5.2.2. Numerical two-phase pressure drop

Concerning the choice of the turbulence model, results of two phase pressure drop predicted by Realizable $k-\varepsilon$ (RKE) and SST $k-\omega$ for NFM are represented in Table 3. Although some Authors (Vallee et al., 2008; and Lo and Tomasello, 2010) obtained that turbulence damping at interface (by the SST $k-\omega$ model) results in a better prediction of the pressure drop, in the present simulations it is the RKE turbulence model to show the best agreement with the experimental data.

Fig. 11 reports the comparison between the concentrated pressure drop from simulations and experiments simulated for both the VFM and NFM in terms of a parity plot. Dashed lines represent ± 15% deviation from bisector because apart from one point, all data fall within ± 15% relative error for both VFM and NFM. Only results using the RKE model are included in this comparison and will be presented in the following sections. The results show a good agreement in both cases, with in general a better agreement for the VFM: maximum relative errors are 11.6% and 16.4% for the VFM and NFM, respectively. It is worth noticing how the simulated two phase pressure drop generally underestimates the actual two phase pressure drop. The higher deviation for the NFM might be due to a poor representation of the more complex flow downstream the sudden expansion: according to visual observations, very often it presents some degree of dispersion.

5.3. Local radial velocity and oil phase holdup

To understand the hydrodynamic behavior of the flow, time-averaged velocity and oil in situ volume fraction (holdup) profiles are evaluated, with reference to VFM cases, along the vertical diameter of a cross section of the upstream pipe at L=0.4 m. Such a distance was selected to ensure that the flow is developed and at the same time that the flow fields are still not affected by the contraction. The results are taken based on time averaging between a period of 4 s and 8 s to ensure that flow fluctuations are removed and steady state conditions are achieved. One core-annular wavy flow and three core-annular flow cases with fixed J_0=0.64 m s^{-1} and variable water superficial velocity are considered. The results for the NFM are not shown here since they practically coincide with the VFM results.

The red solid line and the black dotted lines in Fig. 12 display phase local velocity and oil holdup, respectively. It is evident that the oil core moves with higher velocity than the water adjoining the pipe wall for annular flows. Asymmetric nature of phase and velocity profiles, due to oil buoyancy, is clearly evident, particularly for heavily eccentric cores (Fig. 12a). The velocity profile in the core region shows a piston flow with practically uniform velocity, as expected. Regarding to phase holdup profile, there is an abrupt change of values at the interface, evidencing how the numerical interface is satisfactorily. By increasing water superficial velocity, no significant change in the shape of the velocity profile is observed.

5.4. Cross-section averaged holdup

The already cited Arney correlation (Eq. (3)) was found to predict with very good agreement the water holdup both in ducts having uniform diameter and after sudden changes in the duct section, see e.g. Arney et al. (1993), Colombo et al. (2015). Thus, time-averaged cross sectional water holdup predicted by CFD is plotted versus value obtained using Arney correlation in a parity plot for the VFM and NFM at L=0.4 m from pipe inlet (Fig. 13). The simulated holdup underestimates predictions from the Arney correlation in all cases, with maximum deviation of 16.1% for the VFM and 12.5% for the NFM. Dashed lines of ± 20% are selected; 87% of whole data lies in ± 15%,
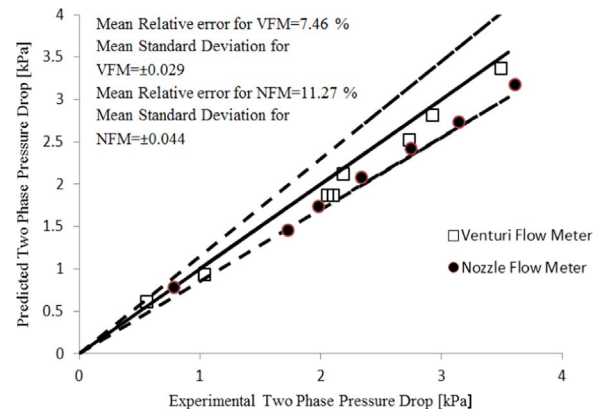

Fig. 11. Comparison between CFD prediction and experimental two-phase concentrated pressure drop. Dotted lines represent ± 15% from the bisector.

a) $J_o = 0.25\ (ms^{-1}), J_w = 0.44\ (ms^{-1})$

b) $J_o = 0.64\ (ms^{-1}), J_w = 0.66(ms^{-1})$

c) $J_o = 0.64\ (ms^{-1}), J_w = 0.88\ (ms^{-1})$

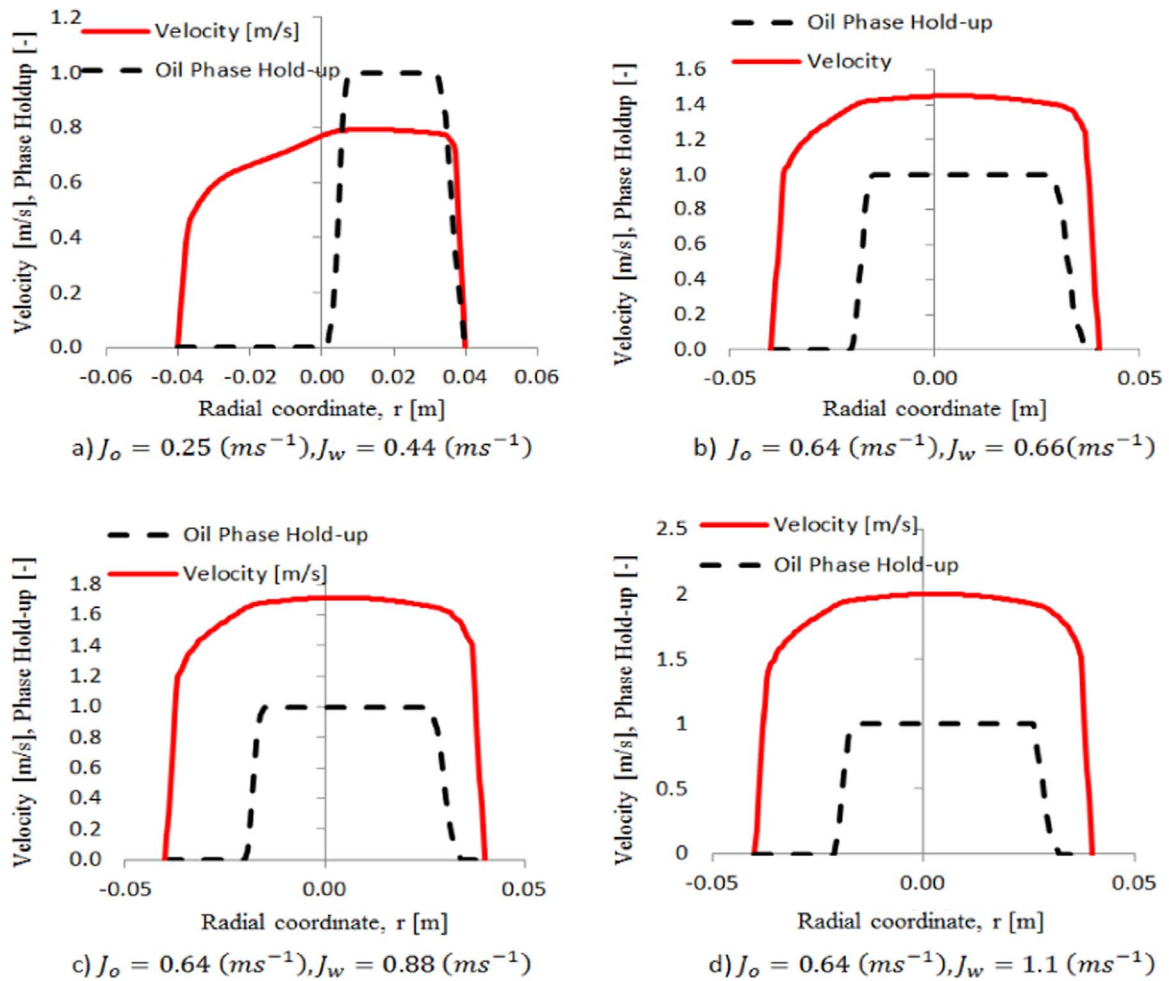d) $J_o = 0.64\ (ms^{-1}), J_w = 1.1\ (ms^{-1})$

Fig. 12. Vertical velocity and local oil fraction (holdup) profiles versus radial coordinate, at L=0.4 m from the inlet. (For interpretation of the references to color in this figure, the reader is referred to the web version of this article.)

while all data falls within ± 20% deviation from bisector. For both devices, regular trends of water holdup are observed as a function of increasing water cut.

Figs. 14 and 15 present cross sectional contour of phase fraction fields at different axial location: upstream pipe (L=0.4 m), throat section (L=0.515 m) and downstream pipe (L=0.612 m) for the VFM and NFM corresponding to J_0=0.51 m s^{-1}, J_w=0.66 m s^{-1} at time instant t=8 s. Due to the fact that gradual and sudden expansion exist

Fig. 13. Parity plot of cross-sectional and time-averaged water holdup from simulation, versus prediction of the Arney et al. (1993) correlation. Dotted lines represent ± 20% from the bisector.

after diffuser for the VFM and NFM, respectively, the axial location at L=0.612 m from the inlet is considered for both devices in CFD model to evaluate the shape of oil core. In both devices, the presence of water layer in the annulus adjacent to the pipe wall is evident. The shape of the oil core evolves from the inlet circular section first towards an elliptic shape and then the lower surface flattens more and more from upstream to downstream of measuring devices. Disturbances and minor deformations of the interface can be observed, as a result of the coarseness of the mesh.
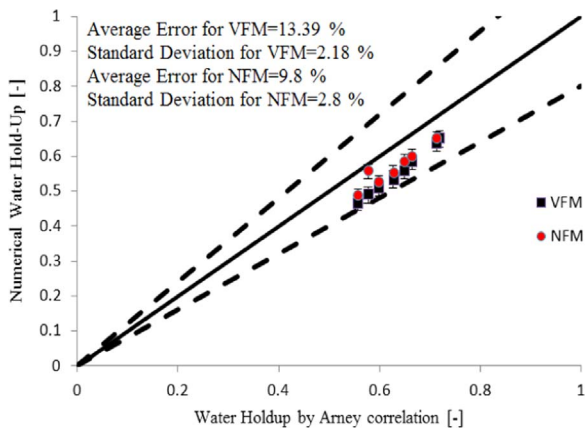
5.5. Slip ratio and two phase mixture velocity

To further investigate the effect of the VFM and NFM on the mixture hydrodynamics, the slip ratio was calculated both in the upstream pipe and at the throat section. Fig. 16 shows the slip ratio as a function of the water holdup at upstream pipe L=0.5 m and throat section L=0.515 m for the VFM case. The average value of slip ratio in the upstream pipe is 0.85 while at throat section it becomes 1.02. Table 4 compares the mean value of slip ratio for both the VFM and NFM, demonstrating the same behavior for the two devices: within them the mixture accelerates, but the acceleration is not uniform between the two fluids. Water accelerates more than oil (as it seems correct, given the higher viscosity of oil) so that the mixture flow becomes practically homogeneous, as it is also found from the experiments. Thus simulations confirm their consistency with the experiments.

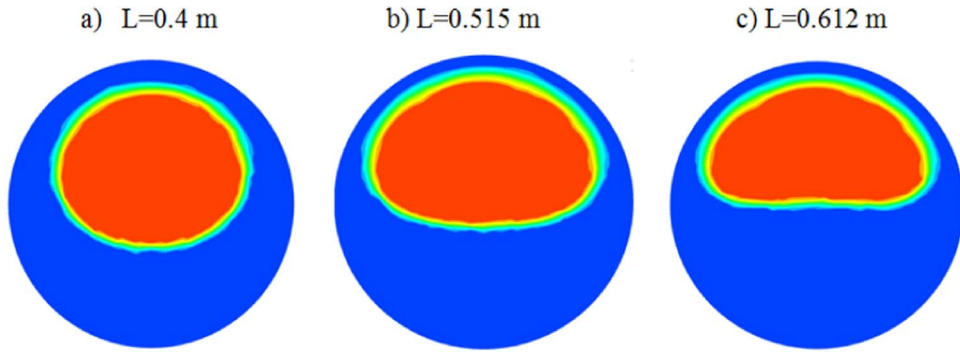In order to calculate the mass flow rate, the value of the discharge

Fig. 14. Cross-sectional oil holdup fields at different axial location for the VFM at time instant t=8 s (color scale is from blue for water to red for oil). (For interpretation of the references to color in this figure legend, the reader is referred to the web version of this article.)

Fig. 15. Cross-sectional oil holdup fields at different axial location for the NFM at time instant t=8 s (color scale is from blue for water to red for oil). (For interpretation of the references to color in this figure legend, the reader is referred to the web version of this article.)
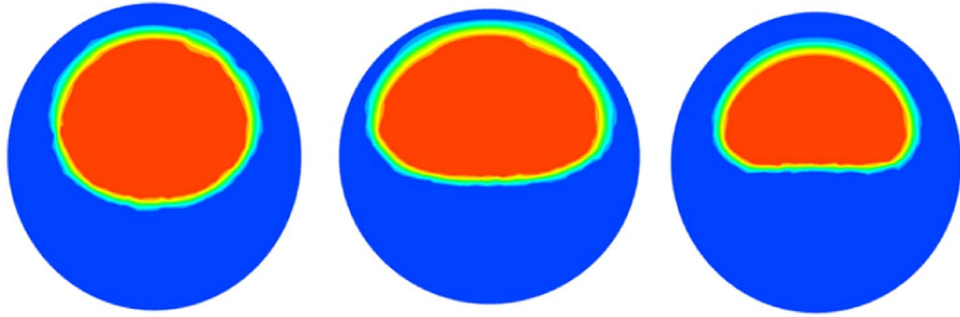
coefficient must be provided (see Appendix B, in particular Eq. (B-1)). For single phase flow, the behavior of the discharge coefficient with the Reynolds number is well known and reported in standards, ISO, 5167-4 (2003) for VFMs and NFMs. However, there is no specific standard for oil-water two phase flow. Hence, the two phase discharge coefficient is calculated from the two phase concentrated pressure drop and mixture density – defined as $\rho = \rho_o H_o + (1 - H_o)\rho_w$ – and correlated with two phase flow Reynolds number developed by Arney et al. (1993), as the flow regime under investigation is core-annular flow:

$$Re_A = \frac{\rho_c D J_{ow}}{\mu_w} \quad [1 + \eta^4(\frac{\mu_w}{\mu_o} - 1)] \tag{4}$$

$$\eta = \sqrt{1 - H_w} \tag{5}$$

Hold up values are taken once again from the Arney correlation. This procedure has been checked in previous works (Sotgia et al., 2008). The resulting average value of discharge coefficients concerning two phase flow and single phase water flow for the VFM and NFM is tabulated in Table 5. Single phase and two-phase flow values of

Fig. 16. Slip ratio obtained from CFD predictions.

discharge coefficient computed from the model are compared with the values suggested by ISO, 5167-4 (2003). Additionally, Fig. 17 depicts the dependence of the two phase flow discharge coefficient on the two phase Reynolds number computed from Eq. (4). It appears that C_d is practically independent of the Reynolds number and that there is minor difference between the VFM and the NFM.

Thanks to the homogeneous behavior of the flow within the devices, a further attempt can be made to obtain the mass flow rate by means of the homogeneous model. After calculation of the discharge coefficient, mass flow rate can be simply obtained by knowing the concentrated pressure drop and the averaged density (computed by Eq. (B-2)). For the simulated cases, the actual flow rates of oil and water are known from experiments, as they were measured by calibrated metering pump and magnetic flow meters, respectively, as reported in Section 4. Fig. 18 reports the comparison between the mass flow rate computed by

Table 4
Simulated mean value of slip ratio upstream pipe and at throat section.

Device	Mean Slip Ratio at Upstream pipe (L=0.5 m)	Mean Slip Ratio at Throat Section (L=0.515 m)
VFM	0.85	1.02
NFM	0.86	1.03

Table 5
Comparison of mean values of discharge coefficient for single and two phase flow.

Measuring devices	Calculated discharge coefficient (single phase water flow, Eq. (B-1))	ISO discharge coefficient (single phase water flow)	Calculated two-phase discharge coefficient (Eq. (B-1))
VFM	0.990	0.97	0.95
NFM	0.92	0.921	0.921

Fig. 17. Two phase discharge coefficient as a function of the Arney Reynolds Number.
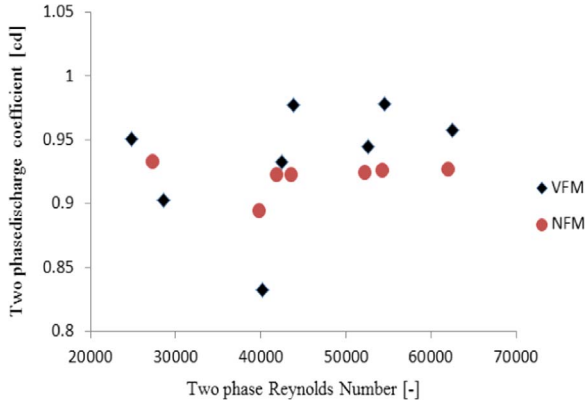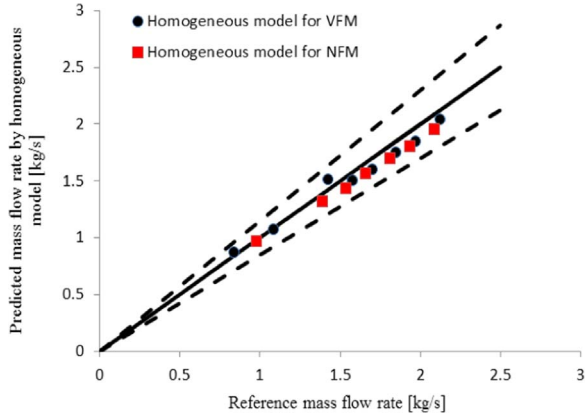

Fig. 18. Parity plot of the comparison between the computed mass flow rate by homogeneous model and reference experimental flow rate. Continuous line evidence the bisector, dashed lines limit ± 15% deviation.

Table 6
Mean relative error and standard deviation between the predicted mass flow rates by using the homogeneous model, and the reference experimental values.

Device	Mean Relative Error (%)	Mean Standard Deviation (%)
VFM	4.4	1.5
NFM	5.5	1.7

homogeneous model with concentrated pressure drop from CFD and the experimental mass flow rate taken as reference. The mean relative error and standard deviation are given in Table 6. In both the VFM and NFM cases simulation results are in good agreement with reference values. This is especially true for the VFM, while the NFM presents a

slightly larger relative error. The dashed lines represent ± 15% deviation from the bisector.

6. Conclusions

Qualitative and quantitative analysis of oil-water mixture through Venturi Flow Meter (VFM) and Nozzle Flow Meter (NFM) were carried out by numerical simulations in the finite volume framework, using the Volume of Fluid (VOF) approach. Mesh dimensions were limited to keep the simulations times relatively short even on common hardware. Simulations have been carried out within a domain discretized with 500,871 mesh elements, that were selected according to a grid independence study. Eight cases of core-annular flow were considered. The core shape could be successfully predicted only in terms of macroscopic characteristics, while the details (e.g. interfacial waves) were not captured, as it could be expected due to the use of RANS turbulence models. Nevertheless, concentrated pressure drop through convergent section of both the VFM and the NFM obtained by simulations showed a very good agreement with respect to experimental pressure drop. Qualitative analysis of velocity in axial direction showed that maximum velocity occurs at throat section and it lasts for a longer distance for NFM than VFM, probably due to presence of abrupt expansion after throat section in case of NFM. Information of two phase pressure drop is important because it can be correlated to mixture velocity: although a separated flow, i.e. core-annular flow regime was observed, the analysis of the slip ratio evidenced that the presence of the VFM and NFM shift the mixture hydrodynamics towards homogeneous flow. To compute the mass flow rate based on homogeneous model, information of two phase discharge coefficient is required, which is generally accepted to be dependent upon Reynolds number. Hence, a new form of two phase Reynolds number based on the work of Arney et al. (1993) was adopted because the flow regime under investigation was core-annular flow. The calculated discharge coefficient was consistent with the values suggested by ISO, 5167-4 (2003). The two phase mixture velocity and the mass flow rate were predicted with satisfactory accuracy (particularly for the VFM) by means of the homogeneous model. Moreover, the results of time-averaged water holdup prediction by CFD were also found to be consistent with the correlation by Arney et al. (1993), which was originally developed for core-annular flows.

The results of the present study thus confirm that CFD is able to offer valuable insight about the flow of oil-water mixtures within these devices. By offering good predictions of the main flow characteristics, even with limited computational requests, it confirms its role as a promising engineering tool in this field. Different design solutions for VFM and NFM (e.g. different convergent and divergent angles) could be tested using CFD, avoiding operational and capital expenditures and reducing the time needed for the development.

Appendix A. Governing parameters for two-phase flow

In this Appendix, a summary of the basic governing parameters for two-phase flows will be presented, as they are the input and the investigated quantities in both the experimental and numerical analysis.

The superficial velocity or volumetric flux of each phase (J, m s^{-1}) is defined as the ratio between the volumetric flow rate and the total cross-sectional area of the pipe:

$$J_o = \frac{Q_o}{A}, \quad J_w = \frac{Q_w}{A} \tag{A-1}$$

Thus, the mixture superficial velocity is obtained as:

$$J_{ow} = \frac{Q}{A} = J_o + J_w \tag{A-2}$$

The input volume fraction ε_w, ε_o (also named water cut and oil cut) are defined as:

$$\varepsilon_w = \frac{J_w}{J_{ow}}, \quad \varepsilon_o = \frac{J_o}{J_{ow}}$$

(A-3)

Superficial Reynolds numbers for the two phases are calculated as:

$$Re_{so} = \frac{\rho_o J_o D}{\mu_o}, \quad Re_{sw} = \frac{\rho_w J_w D}{\mu_w}$$

(A-4)

Concerning the distribution of the phases within the duct, the first quantity of interest is the state density function of the ith phase $\alpha_i(p,\tau)$, a local, instantaneous, Boolean quantity defined as 1 if at instant τ point p is immersed in the ith phase, 0 otherwise.

The time average of the state density function gives the local holdup H_{wp}, which in its turn can be averaged on chords, cross-sections and volumes extracted from the pipe. Both local and cross-sectional holdup H will be used in the analyses presented in the following.

For two-phase flows, the holdup of one phase is obviously the complement to unity of the other one, e.g. $H_o = 1 - H_w$.

Effective (actual) velocity of each phase can be correlated to the superficial velocity as:

$$U_w = \frac{J_w}{H_w}; U_o = \frac{J_o}{H_o}$$

(A-5)

Finally, the slip ratio is defined as the ratio between the effective velocities of the phases:

$$S = \frac{U_w}{U_o} = \frac{J_w}{J_o} \frac{(1-H_w)}{H_w}$$

(A-6)

Thus, information on holdup plays an important role in the characterization of two phase flows.

Appendix B. Theory of differential pressure devices

In subsonic flows when a fluid passes through a convergent section of a pipe the mass flux has to increase. In absence of work and heat exchanges with the surroundings, this causes a pressure decrease, that can be related to the mass flow rate:

$$Q_m = \frac{C_d}{\sqrt{1-\beta^4}} \cdot \varepsilon \cdot \frac{\pi}{4} \cdot d^2 \cdot \sqrt{2 \ \Delta P \rho}$$

(B-1)

where Q_m, β and d are the mass flow rate, diameter ratio (throat/upstream) and throat diameter, respectively. ΔP is the pressure drop measured from upstream pipe to throat section. The discharge coefficient C_d correlates actual to ideal flow rates, to account for the effects of turbulence and flow separation, therefore it is usually related to the Reynolds number. To take into account effect of compressibility of fluids, the expansibility factor ε is also introduced: for incompressible fluids it can be 1, while for gas flow $\varepsilon < 1$. The numerical values of both C_d and ε for use in measurement devices are tabulated in ISO5167-4 (2003).

The same model can be used for mixture flows across converging devices, but in this case mixture density has to be specified according to a suitable model. The easiest model is the homogeneous model, which is based on the assumption that the two components move with the same velocity (i.e., slip ratio is unity). In this case the volume averaged holdup and the input volume fraction coincide and the mixture density can be expressed as:

$$\rho_m = \ \varepsilon_w \rho_w + (1 - \varepsilon_w) \rho_o$$

(B-2)

So, using Eqs. (B-1) and (B-2) and measuring ΔP, the mass flow rate of the mixture can be obtained.

Appendix C. The volume of fluid model

Basic equations

By assumptions of no mass exchange between the phases and incompressible flow, the partial differential equations for mass and momentum conservation are, respectively:

$$\nabla \cdot (\vec{U}) = 0$$

(C-1)

$$\frac{\partial}{\partial t}(\vec{U}) + \nabla \cdot \ (\vec{U}\vec{U}) = -\nabla P + \nabla \cdot \left[\mu \left(\nabla \vec{U} + \nabla \vec{U}^T \right) \right] + \rho \vec{g} + \vec{F}$$

(C-2)

where $\vec{U}, \mu$, P , $\vec{g}$ and $\vec{F}$ are velocity field, viscosity, pressure, gravity vector and the contribution to the body force related to surface tension force, as it will be detailed in the following. Unlike Eulerian-Eulerian two-fluid methods, that solve a momentum equation for each of the phases, in VOF a unique momentum equation is shared for both phases, with density and viscosity calculated on the basis of the volume fractions of the phases. The amount of the secondary phase (in the present case, oil) in each computational cell is in fact calculated by tracking the state density function (α_o) for such phase (that is why VOF belongs to the family of volume tracking techniques). As the phase density is constant, this is equivalent to solving the continuity equation for the single phase:

$$\frac{\partial(\rho_o \alpha_o)}{\partial t} + \ \nabla \cdot (\rho_o \alpha_o \vec{U}) = 0$$

(C-3)

In presence of only two phases, the volume fraction of the primary phase is obviously the complement to unity of the previous, exactly as in the physical world.

Once the volume fractions of the phases are calculated in each computational cell, average properties in the cell are estimated as:

$$\rho = \rho_o \alpha_o + (1 - \alpha_o)\rho_w$$
$$\mu = \mu_o \alpha_o + (1 - \alpha_o)\mu_w \qquad \text{(C-4)}$$

Interface tracking

Within the computational domain, cells were oil holdup α_o is 0 are cell filled with water, while the value $\alpha_o = 1$ is associated with the cells fully filled with oil. A value between 0 and 1 occurs at interface cells. From the set of interface cells, the interface shape has to be reconstructed using a suitable algorithm, as with all volume tracking – interface capturing methods. In the present study, the geometric reconstruction piecewise-linear scheme is used. It assumes that the interface between the two phases is planar within each cell and, based on this linear interface representation the normal and tangential velocity distributions, the derivatives of the phase volume fractions and the advection of fluids through each cell are calculated. Finally, phase volume fraction is updated using balances of fluxes calculated in the previous step.

Surface tension

In the VOF method, addition of the surface tension results in an extra source term in the momentum equation. In the present study, the Continuum Surface Force (CSF) model by Brackbill et al. (1992) was used.

By assumption of constant surface tension along the interface, the well-known Laplace-Young equation holds, and the source term can be defined as:

$$\vec{F} = \sigma k \frac{\rho \nabla \alpha_o}{0.5 \ (\rho_o + \rho_w)} \qquad \text{(C-5)}$$

where σ, k, and $\nabla \alpha_o$ are surface tension, interface curvature and the oil phase volume fraction gradient, respectively. In the CSF model the surface curvature is calculated based on the local gradient of the vector normal to the interface, defined as the gradient of the volume fraction of oil α_o:

$$n = \nabla \alpha_o \quad , \quad \hat{n} = \frac{n}{|n|} \text{ and } k = \nabla . \hat{n} \qquad \text{(C-6)}$$

References

Angeli, P., Hewitt, G.F., 2000. Flow structure in horizontal oil-water flow. Int. J. Multiph. Flow 26, 1117–1140.

ANSYS Fluent Theory Guide 16.2., 2015

Arney, M.S., Bai, R., Guevara, E., Joseph, D.D., Liu, K., 1993. Friction factor and holdup studies for lubricated pipelining- I Experiments and correlations. Int. J. Multiph. Flow 19, 1061–1076.

Atkinson, I., Berard, M., Conort, G., Groves, J., Lowe, T., McDiarmid, A., Mehdizade, P., Perciot, P., Pinguet, B., Smith, G., Williamson, K.J., Winter 2004/2005. A New Horizon in Multiphase Flow Measurement. Retrieved from ⟨http://www.slb.com/resources/publications⟩.

Brackbill, J.U., Kothe, D.B., Zemach, C., 1992. A continuum method for modeling surface tension. J. Comput. Phys. 100, 335–354.

Brauner, N., 1991. Two-phase liquid-liquid annular flow. Int. J. Multiph. Flow 17, 59–76.

Charles, M.E., Govier, G.T., Hodgson, G., 1961. The horizontal pipeline flow of equal density oil-water mixtures. Can. J. Chem. Eng. 39 (1), 27–36.

Chisholm, D., 1967. Pressure gradients during the flow of incompressible two-phase mixtures through pipes, venturis and orifice plates. Br. Chem. Eng. 12, 454–457.

Colombo, L.P.M., Guilizzoni, M., Sotgia, G.M., 2012. Characterization of the critical transition from annular to wavy-stratified flow for oil-water mixtures in horizontal pipes. Exp. Fluids 53, 1617–1625.

Colombo, L.P.M., Guilizzoni, M., Sotgia, G.M., Marzorati, D., 2015. Influence of sudden contractions on in situ volume fractions for oil-water flows in horizontal pipes. J. Heat Fluid Flow 53, 91–97.

Desamala, A.B., Vijayan, V., Dasari, A., Dasmahapatra, A.K., Mandal, T.K., 2016. Prediction of oil-water flow patterns, radial distribution of volume fraction, pressure and velocity during separated flows in horizontal pipe. J. Hydrodyn. Ser. B 28 (4), 658–668.

Falcone, G., Hewitt, G., Alimonti, C., 2009. Multiphase Flow Metering, Principles and Applications 1st edition. Elsevier Science - Developments in Petroleum Science, Oxford UK.

Ghosh, S., Das, G., Das, P.K., 2010. Simulation of core annular downflow through CFD – a comprehensive study. J. Chem. Eng. Process. 49, 1222–1228.

Gordon, D., 2012. Understanding Unconventional Oil, The Carnegie papers, Energy and climate, 2012. (available online at ⟨http://carnegieendowment.org/files/unconventional_oil.pdf⟩).

Hirt, C.W., Nichols, B.D., 1981. Volume of fluid (VOF) method for the dynamics of free boundries. J. Comput. Phys. 39, 201–225.

IEA International Energy Agency, 2013. Resources to Reserves 2013. (available online at: ⟨http://www.iea.org/publications/freepublications/publication/Resources2013. pdf⟩).

ISO 5167-4, 2003. Measurement of Flow Fuel by Means of Pressure Differential Devices Inserted in Circular Cross-section Conduits Running Full – Part 4: Venturi Tubes.

Issa, R., 1986. Solution of the implicitly discretized fluid flow equations by operator splitting. J. Comput. Phys. 62, 40–65.

Jana, A.K., Das, G., Das, P.K., 2008. The hydrodynamics of liquid-liquid upflow through a venturimeter. Int. J. Multiph. Flow 34, 1119–1129.

Joseph, D., Renardy, Y., 1993. Fundamentals of Two-Fluid Dynamics. Springer, New York US.

Joseph, D., Bai, R., Chen, K.P., Renardy, R., 1997. Core annular flows. Annu. Rev. Fluid Mech. 29, 65–90.

Kaushik, V.V.R., Ghosh, S., Das, G., Das, P.K., 2012. CFD simulation of core annular flow through sudden contraction and expansion. J. Pet. Sci. Eng. 86–87, 153–164.

Leeuw, Rd, 1997. Liquid Correction of Venturimeter Reading in Wet Gas Flow. North Sea Flow Measurement Workshop, Kristiansand, Norway.

Li, X., Huang, Z., Meng, Z., Wang, B., Li, H., 2009. Oil-water two phase flow measurement using a venturi meter and an oval gear flow meter. Chem. Eng. Commun., 223–231.

Lo, S., Tomasello, A., 2010. Recent Progress in CFD Modelling of Multiphase Flow in Horizontal and Near-horizontal Pipes. 7th North American Conference on Multiphase Technology, Banff, Canada.

Menard, T., Tanguy, S., Berlemont, A., 2007. Coupling level set/VOF/ghost fluid methods: validation and application to 3D simulation of the primary break-up of a liquid jet. Int. J. Multiph. Flow 33, 510–524.

NFOGM, 2005. Handbook of Multiphase Flow Metering, Revision 2, 2005, The Norwegian Society for Oil and Gas Measurement and The Norwegian Society of Chartered Technical and Scientific Professionals. (available online at: ⟨http://nfogm. no/wp-content/uploads/2014/02/MPFM_Handbook_Revision2_2005_ISBN-82-91341-89-3.pdf⟩).

Oddie, G., Pearson, J.R.A., 2004. Flow rate measurement in two-phase flow. Sclumberger Camb. Res..

Oliemans, R., Ooms, G., 1986. Core annular flow of oil and water through a pipeline. In: Hewitt, G.F., Delhaye, J.M., Zuber, N. (Eds.), Multiphase Science and Technology. Hemisphere Publishing Corp., Washington, 2.

Oliemans, R.V.A., Ooms, G., LWu, H., Duijvestjn, A., 1987. Core-annular oil/water flow: the turbulent-lubricatinf-film model and measurements in a 5 cm pipe loop. Int. J. Multiph. Flow, 23–31.

Oliveira, J.L.G., Passos, J.C., Verschaeren, R., Van der Geld, C., 2009. Mass flow rate measurements in gas-liquid flows by means of a venturi or orifice plate coupled to a void fraction sensor. Exp. Therm. Fluid Sci. 33 (2), 253–260.

Ooms, G., Segal, A., Van Der Wees, A.J., Meerhoff, R., Oliemans, R.V.A., 1984. A theoretical model for core-annular flow of a very viscous oil core and water annulus through a horizontal pipe. Int. J. Multiph. Flow 10, 41–60.

Pal, R., 1993. Flow of oil-in-water emulsions through orifice and venturi meters. Ind. Eng. Chem. Res. 32, 1212–1217.

Patankar, S., 1980. Numerical Heat Transfer and Fluid Flow. Washington DC.

Ranade, V.V., 2002. Computational Flow Modeling for Chemical Reactor. Engineering Bath: Academic Press.

Saniere, A., Hénaut, I., Argillier, J.F., 2004. Pipeline Transportation of Heavy Oils, a

Strategic, Economic and Technological Challenge, Oil & Gas Science and Technology – Rev. IFP. vol. 59(5). pp. 455–466.

Skea, A.F., Hall, A.W.R., 1999. Effects of water in oil and oil in water on single-phase flowmeter. Flow Meas. Instrum. 10, 151–157.

Sotgia, G., Tartarini, P., Stalio, E., 2008. Experimental analysis of flow regimes and pressure drop reduction in oil-water. Int. J. Multiph. Flow, 1161–1174.

Tan, C., Dong, F., 2010. Modification to mass flow rate correlation in oil-water two phase flow by a V-cone flow meter in consideration of the oil-water viscosity ratio. Meas. Sci. Technol., 21.

Vallee, C., Hohne, T., Prasser, H.-M., Suhnel, T., 2008. Experimental investigation and CFD simulation of horizontal stratified two-phase flow phenomena. Nucl. Eng. Des. 238 (3), 637–646.

Varsteeg, H.K., Malalasekera, W., 1995. Introduction to Computational Fluid Fynamics – The Finite Volume Method. Longman Scientific and Technical, Essex, England.